Preprints.org

Article

Not peer-reviewed version

Absence of Weak Localization Effects in Strontium Ferromolybdate

Gunnar Suchaneck * and Evgenii Artiukh

Posted Date: 16 May 2023

doi: 10.20944/preprints202305.1081.v1

Keywords: Strontium ferromolybdate; electrical conductivity; weak localization

Preprints.org is a free multidiscipline platform providing preprint service that is dedicated to making early versions of research outputs permanently available and citable. Preprints posted at Preprints.org appear in Web of Science, Crossref, Google Scholar, Scilit, Europe PMC.

Copyright: This is an open access article distributed under the Creative Commons Attribution License which permits unrestricted use, distribution, and reproduction in any medium, provided the original work is properly cited.

Preprints (www.preprints.org) | NOT PEER-REVIEWED | Posted: 16 May 2023 doi:10.20944/preprints202305.1081.v1

Disclaimer/Publisher's Note: The statements, opinions, and data contained in all publications are solely those of the individual author(s) and contributor(s) and not of MDPI and/or the editor(s). MDPI and/or the editor(s) disclaim responsibility for any injury to people or property resulting from any ideas, methods, instructions, or products referred to in the content.

Article

Absence of Weak Localization Effects in Strontium Ferromolybdate

Gunnar Suchaneck [1,*] and Evgenii Artiukh [2]

[1] TU Dresden, Institute of Solid-State Electronics, Dresden Germany; gunnar.suchaneck@tu-dresden.de
[2] SSPA "Scientific-Practical Materials Research Centre of NAS of Belarus", Cryogenic research division, 220072 Minsk, Belarus; sirfranzferdinand@yandex.ru
* Correspondence: gunnar.suchaneck@tu-dresden.de; Tel.: +49 351 46335281

Abstract: $Sr_2FeMoO_{6-\delta}$ (SFMO) double perovskite is a promising candidate for room-temperature spintronic applications since it possesses a half-metallic character (with theoretically 100% spin polarization), a high Curie temperature of about 415 K, and a low-field magnetoresistance (LFMR). However, due to different synthesis conditions of ceramics as well as thin films, different mechanisms of electrical conductivity and magnetoresistance prevail. In this work, we consider the weak localization effect in SFMO occurring in disordered metallic or semiconducting systems at very low temperatures due to quantum interference of back-scattered electrons. We calculate the quantum corrections to conductivity and the contribution of electron scattering to the resistivity of SFMO. We attribute the temperature dependence of SFMO ceramics resistivity in the absence of a magnetic field to the fluctuation induced tunneling model. Also, we attribute the decreasing resistivity in the temperature range from 409 K up to 590 K to adiabatic small polaron hopping and not to localization effects. Both fluctuation induced tunneling and adiabatic small polaron hopping do not favor quantum interference. Additionally, we demonstrate that the resistivity upturn behavior of SFMO cannot be explained by weak localization. Consequently, to the best of our knowledge, there is still no convincing evidence for the presence of weak localization in SFMO.

Keywords: strontium ferromolybdate; electrical conductivity; weak localization

1. Introduction

In a disordered electronic system, the electron motion is diffusive due to scattering at non-uniformities. Weak localization is a physical effect which occurs in disordered electronic systems at very low temperatures. The effect manifests itself as a correction Ds to the conductivity (or correspondingly the resistivity) of a metal or semiconductor arising in the case that the mean free path l is in the order of the wavelength $\lambda_F = 2\pi/k_F$ of the carrier wavefunctions, i.e. $k_F l \sim 1$, with k_F denoting the Fermi wave vector. The weak localization correction comes from quantum interference of back-scattered electrons. Labeling all the trajectories by the time t it takes for a classical particle to go around a loop, the classical probability dP that the diffusing particle returns into the phase volume dV at a given time t is given by [1] (p. 153)

$$dP = \frac{dV}{(4\pi Dt)^{d/2}} \tag{1}$$

where P is the probability for a quantum mechanical particle to return to the starting point (the wave function of both time-reversed paths will constructively interfere with each other), $D = v_F^2 t/d$ is the diffusion constant, t is the elastic scattering time and d is the dimension. The relevant phase volume can be estimated as $v_F\, dt\, (\delta\rho\delta\varphi)^{d-1}$[2,3], where $v_F = (2E_F/m_e)^{1/2}$ is the Fermi velocity, E_F the Fermi energy, m_e the electron mass, $\delta\rho$ and $\delta\varphi$ characterize the transverse distance between the electron trajectories 1 and 2 at the intersection point and $\delta\varphi$ is the intersection angle between the both trajectories. For the interference between paths 1 and 2 to be effective, the uncertainty relation should hold

© 2023 by the author(s). Distributed under a Creative Commons CC BY license.

Preprints (www.preprints.org) | NOT PEER-REVIEWED | Posted: 16 May 2023 doi:10.20944/preprints202305.1081.v1

$$p_F \delta\rho\delta\phi = \hbar k_F \delta\rho\delta\phi = h \tag{2}$$

where $p_F = m_e v_F$ is the Fermi momentum and h the Planck constant. This leads to a relative change in conductivity of two and three dimensional systems yielding [1] (p. 183):

$$\frac{\delta\sigma_{2D}}{\sigma_0} = -\frac{2}{\pi k_F l_e}\ln\frac{l_\Phi}{l_e}, \qquad \frac{\Delta\sigma_{3D}}{\sigma_0} = -\frac{3}{2(k_F l_e)^2} \tag{3}$$

where σ_0 is the residual low temperature conductivity taken as the Drude conductivity, i.e. $\sigma_D = e^2 n_e t_e/m_e$, determined by relaxation time t of the dominating charge scattering mechanism, the electron charge e, the electron density n_e, the elastic scattering time τ_e and the electron mass m_e. In eq. (3), the negative sign is due to the fact that the returning trajectory should arrive at the intersection point with the momentum almost opposite to the initial one. This means that interference lowers the conductivity. Note that for small sizes b the volume $(Dt)^{d/2}$ should be replaced by $(Dt)^{d/2}b^{3-d}$ since the charge carrier has a chance to diffuse repeatedly from one wall to the other and the probability of finding it at any point across films or wires limited in size will be the same [4]. However, we are considering macroscopic sizes rather than sizes of the order of atomic distances. The lower cutoff τ_e is justified with the fact that within a time τ_e no elastic scattering occurs, and therefore there will be no closed trajectories. The upper limit is given by [5]:

$$\tau_\Phi^{-1} \sim \left(\frac{T}{D^{d/2} N_0 a^{3-d}}\right)^{2/(4-d)}, \tag{4}$$

where $D = (v_F^2 t_e/d)$ is the diffusion constant, N_0 is the one-spin density of states, d the characteristic sample dimension. The phase coherence time t_ϕ defines the phase coherence length $l_\phi = (Dt_\phi)^{1/2}$. This yields conductivity corrections for two and three dimensional systems amounting in terms of quantum conductance e^2/h to [1] (p. 282):

$$\Delta\sigma_{2D} = -\frac{2e^2}{\pi h}\ln\frac{l_\varphi}{l_e} = -\frac{e^2}{\pi h}\ln\left(\frac{l_\varphi}{l_e}\right)^2, \qquad \Delta\sigma_{3D} = -\frac{e^2}{\pi h}\left(\frac{1}{l_e} - \frac{1}{l_\varphi}\right), \tag{5}$$

with l_e the mean free path of the electron.

Temperature modifies the phase coherence length l_ϕ and, therefore, modifies the weak localization correction. The temperature dependence of l_φ can be described as [6,7]

$$\frac{1}{l_\phi^2(T)} = \frac{1}{l_\phi^2(0)} + A_{ee}T^{p_1} + A_{ep}T^{p_2}, \tag{6}$$

where $l_\varphi(0)$ is the zero-temperature phase coherence length and $A_{ee}T^{p1}$ and $A_{ep}T^{p2}$ represent the contributions from two different dephasing mechanisms, e.g. electron-electron (ee) and electron-phonon (ep) interactions, respectively. Note that the temperature exponents p_1 and p_2 changes fundamentally with the system dimensionality [8]. If electron-electron interaction is the dominant dephasing mechanism (also denoted as Nyquist dephasing mechanism), this gives rise to $\tau_{ee} \propto T^{-p}$ with values of p equal to 0.66, and 1 for $d = 1$ and $d = 2$, respectively [1] (chapter 13.6.4), [5]. For $d = 3$ eq. (4) yields $p = 2$ while the result in [1] (p. 509) is $p = 1.5$. The electron-phonon interaction decoherence mechanism would provide a temperature dependence of the dephasing time $t_\phi \propto T^{-3}$ [9]. Typically, one finds $\tau_\varphi \approx \tau_{ep} \propto T^{-p}$ with the exponent of temperature $p \approx 2$–4.

Preprints (www.preprints.org) | NOT PEER-REVIEWED | Posted: 16 May 2023 doi:10.20944/preprints202305.1081.v1

In metals and semiconductors at low temperatures, quasielastic (small energy transfer) electron-electron scattering is the dominant dephasing process. Assuming only one dephasing process and accounting that $l_\varphi(0)$ is in the order of 50 nm to several micrometers, that is, usually $l_\varphi(0) >> l_\varphi(T)$ [6,7,10–12], a simplified approximation formula is given by [11]:

$$\frac{1}{l_\phi^2(T)} \approx A'T^{p_1}, \tag{7}$$

with $p_1 = 1$ for quasielastic electron-electron scattering in agreement with experimental results in Bi_2Te_3 thin films [13], 50 nm-thick Cd_3As_2 films [11], Bi_2Te_3 single crystals [7], $Mo_xW_{1-x}Te_{2+d}$ ultrathin films [14]. As a result, we obtain for quasi-elastic electron-electron scattering:

$$l_\varphi^2 = l_\varphi^2(T_0)\cdot\frac{T_0}{T}, \tag{8}$$

Consequently, eq. (5) transforms to

$$\Delta\sigma_{2D,WL} = -\frac{e^2}{\pi h}\ln\left(\frac{l_\phi^2(T_0)}{l_e^2}\cdot\frac{T_0}{T}\right) = \frac{e^2}{\pi h}\ln\left(\frac{l_e^2}{l_\phi^2(T_0)}\cdot\frac{T}{T_0}\right) =$$
$$= \frac{e^2}{\pi h}\left[\ln\left(\frac{l_e^2}{l_\phi^2(T_0)}\right)+\ln\left(\frac{T}{T_0}\right)\right] \tag{9}$$
$$\delta\sigma_{3D,WL} = -\frac{e^2}{\pi}\left(\frac{1}{l_e}-\frac{1}{l_\phi}\right) = -\frac{e^2}{\pi\cdot l_e}+\frac{e^2}{\pi\cdot l_\phi(T_0)}\left(\frac{T}{T_0}\right)^{1/2}$$

Finally, the total conductivity consisting of 2D at high magnetic fields and 3D contributions is written as:

$$\sigma(T) = \sigma_0 + A\cdot\ln\left(\frac{T}{T_0}\right)+B\cdot\left(\frac{T}{T_0}\right)^{1/2}, \tag{10}$$

with

$$\sigma_0 = \sigma_D - \frac{e^2}{\pi hb}\cdot\ln\left(\frac{l_\phi^2(T_0)}{l_e^2}\right)-\frac{e^2}{\pi h\cdot l_e}, \tag{11}$$

and the coefficients:

$$A = \frac{e^2}{\pi hb},\quad B = \frac{e^2}{\pi h\cdot l_\phi(T_0)}, \tag{12}$$

where b is the effective thickness of the 2D layer introduced to convert a 2D conductivity to a 3D one. A minimum of conductivity appears only when the second right-side term in Equation (10) changes sign, i.e.:

$$B = -\frac{2A}{(T_{max}/T_0)^{1/2}}\underset{T_0=T_{max}}{=} -2A, \tag{13}$$

With regard to Equation (10), quantum correction to residual conductivity may be written as [15]:

$$\Delta\sigma(T) = A'T + B'T^{1/2}, \tag{14}$$

Preprints (www.preprints.org) | NOT PEER-REVIEWED | Posted: 16 May 2023 doi:10.20944/preprints202305.1081.v1

Assuming that Mathiessen's rule holds, and representing resistivity as a sum of elastic and inelastic contributions where the latter increase with increasing temperature due to a power law (e.g. a term CT^n), the resistivity data can be be fitted to [16,17]:

$$\rho(T) = \frac{1}{\sigma_0 + A' \ln T + B' T^{1/2}} + C_n T^n, \qquad (15)$$

with n equal to 3/2, 2, 3, depending on the dominant scattering mechanism [18].

Separate conductivity quantum correction terms in the form $A' \ln T$ and $B' T^{1/2}$ were introduced for $La_{0.7}Ca_{0.3}MnO_3$ by Kumar et al [19]. Here, the first term $A' \ln T$ was attributed also to the Kondo effect [20]. In order to account for higher order scattering mechanisms and to extend the analytical description to higher temperatures, an additional term CT^n was included. The electron-electron interaction term $B' T^{1/2}$ was applied also to $La_{0.7-x}Y_xSr_{0.3}MnO_3$ ($0 \le x \le 0.2$) ceramics of 1 mm thickness [21], to $La_{0.7}A_{0.3}MnO_3$ (A=Ca,Sr,Ba) ceramics [22], to $La_{0.6}Re_{0.1}Ca_{0.3}MnO_3$ (Re = Pr, Sm, Gd, Dy) ceramics of 1 mm thickness all three prepared by conventional solid state reaction [23], to $SrRuO_3$ thin films with a thickness of 6 to 8 nm deposited by pulsed laser deposition onto (100)$SrTiO_3$ substrates [16], to ultrathin $La_{0.7}Sr_{0.3}MnO_3$ films (3.5 to 40 nm), deposited by molecular beam epitaxy [17], and to metallic $SrRuO_3$ and $LaNiO_3$ thin films deposited by pulsed laser deposition with a thickness of 6 and 240 nm, respectively [24].

In the $La_{0.7}Sr_{0.3}MnO_3$ ultrathin film case, a crossover from $T^{1/2}$ to a $\ln T$ behavior in the low-temperature resistivity dependence with decreasing thicknesses was related to a change in the dimensionality of the system, going from 3D for samples thicker than 20 nm to 2D in the limit of ultrathin samples. The origin of this effect is that in the case of a film thickness larger than the Landau orbit length $L_H = (\hbar/2eB)^{1/2}$ the system behaves essentially as 3D while in the opposite electron confinement results in a 2D behavior of the system. In the 3D case of metallic and ferromagnetic $SrRuO_3$ and of metallic and paramagnetic $LaNiO_3$ epitaxial thin films the term $B' T^{1/2}$ was spitted into two terms where in the 3D case first term $b_1 T^{p/2}$ accounts for the weak localization and the $b_2 T^{1/2}$ term stands for the renormalized electron-electron interaction quantum corrections [25]. In the 2D case, both these quantum corrections to conductivity have a similar temperature dependence. Here, only a $\ln T$ term remains. The quantum correction of conductivity in metallic $LaNi_{1-x}Co_xO_3$ ($0 \le x \le 0.75$) below 2 K follows a power law BT^m where away from the metal-insulator transition ($x \le 0.4$) m takes a value of m = 0.3…0.4. Such power-law conductivities are seen at the metallic side of the metal-insulator transition also for other ABO_3 oxides [26].

In this work, we attribute the temperature dependence of the SFMO ceramic resistivity in the absence of a magnetic field to the fluctuation induced tunneling model and the decrease of resistivity in the temperature range from 409 K up to 590 K not to localization effects but to adiabatic small polaron hopping. Both fluctuation induced tunneling and adiabatic small polaron hopping do not favor quantum interference. Also, we demonstrate that the resistivity upturn behavior of SFMO cannot be explained by the weak localization effect.

2. Methods

First we estimate the coefficient A' in Equation (15). Taking $l_F < 0.46$ nm at room temperature [27] and b = 20 nm [17], the ratio of the coefficients A'/B' will be in the order of 10^{-2}. Since for arguments larger than one the natural logarithm function will be smaller than the root function, the logarithmic term can be neglected. A further indication of small A' coefficients arises from the depth of the conductance minimum, i.e. the difference $r(0)$-$r(T_{min})$, which changes with increasing magnetic flux [19]. Values of above 35 mW·cm in the absence of a magnetic field down to 2.4 mW·cm at 7 T [28] yield coefficients $A' = 10^{-2} \cdot (r(0)\text{-}r(T_{min}))$ [20,29]. In $La_{0.7}Sr_{0.3}MnO_3$ ultrathin films (3.5 to 40 nm), deposited by molecular beam epitaxy [17], the agreement of fits of conductivity data to equation (15) with only the $A' \ln T$ term ($B' = 0$) was much worse than in the case with only the $B' T^{1/2}$ term ($A' = 0$). Therefore, we neglect in the following the term $A' \ln T$. This corresponds to the common practice of describing similar materials like $La_{0.7-x}Y_xSr_{0.3}MnO_3$ ($0 \le x \le 0.2$) ceramics of 1 mm thickness prepared by conventional solid state reaction [21], $La_{0.7}A_{0.3}MnO_3$ (A=Ca,Sr,Ba) ceramics prepared by

Preprints (www.preprints.org) | NOT PEER-REVIEWED | Posted: 16 May 2023 doi:10.20944/preprints202305.1081.v1

conventional solid state reaction [22], and $SrRuO_3$ thin films with a thickness of 6 to 8 nm deposited by pulsed laser deposition onto (100)$SrTiO_3$ substrates [16].

The coefficient B' is given by [15]:

$$B' = .0309\frac{e^2}{\hbar}\cdot\sqrt{\frac{k}{\hbar D}} = \frac{2.72149\cdot\Omega^{-1}\mathrm{K}^{-1/2}\mathrm{s}^{-1/2}}{\sqrt{D[\mathrm{m}^2/\mathrm{s}]}}. \quad (16)$$

with $\hbar = h/2p$ the Planck constant expressed in J s radian^{-1}. For a mean free path l_e of 0.46 nm at room temperature [27] and a carrier relaxation time t of 1.6×10^{-14}s [30], the carrier diffusion constant will be 1.32×10^{-5} m^2 s^{-1} yielding a coefficient $B' \approx 748$ W^{-1} m^{-1} K$^{-1/2}$ in satisfactory agreement with values of $B' \approx$ 360…500 W^{-1} m^{-1} K$^{-1/2}$ in in $(Ni_{0.5}Zr_{0.5})_{1-x}Al_x$ metallic glasses [31] and with a universal value of $B' \approx 600$ W^{-1} m^{-1} K$^{-1/2}$ of amorphous and disordered metals [32]

The coefficient C_n was calculated as follows: We start with Drude conductivity:

$$\rho_D = \frac{\hbar k_F}{n_e e^2 l_e}, \quad (17)$$

where n_e the electron density and e the electron charge. Taking $n_e = 1.1\times10^{28}$ m^{-3} [33] we obtain $\hbar k_F = 4.8\cdot10^{-25}$ Jsm^{-1} and

$$\rho_D = \frac{1.87\cdot10^{-15}\Omega\mathrm{m}}{l_e[\mathrm{m}]}, \quad (18)$$

We assume electron mean free paths l_e = 0.46 nm and 1.11 nm at room temperature and 4 K, respectively, calculated from the ordinary Hall coefficient [27]. This yields r_D = 4.07 μWm at room temperature and r_D = 1.68 μWm at 4 K in satisfactory agreement with experimental data of single crystal SFMO in [34]. Now we assume that in a ferromagnetic state below room temperature magnetic scattering controls electrical transport in SFMO at low temperatures [27]. The mean free path of electron scattered by a spin wave with energy E_s travelling through the bcc I4/mmm lattice in thermal equilibrium at a temperature T, is given by [35]:

$$l_e = \frac{S^2V^{1/3}\theta^{-7/2}}{\pi\zeta(3/2)(E_\sigma/kT)} \approx 0.38\cdot S^{9/2}a\cdot\left(\frac{J}{kT}\right)^{5/2}, \quad (19)$$

where S is the effective spin $S_{eff} = (S_{Fe}S_{Mo})^{1/2} = (1/2\cdot5/2)^{1/2} = 1.118$, V the unit cell volume, q a dimensionless temperature, z the Rieman Zeta function, a the lattice constant, and J the exchange constant of the 180° Fe-O-Fe interaction amounting to -25 K [36,37]. Finally, we arrive at:

$$\rho_D = 2.413\cdot10^{-9}\cdot T^{5/2}\Omega\mathrm{m}, \quad (20)$$

Compared to the experimental value of $R_{2.5} = 1.4\times10^{-11}$ WmK$^{-5/2}$ in a relation $r = r_0 + R_{2.5}T^{2.5}$ the calculated value of $R_{2.5}$ is overestimated by almost two orders of magnitude in part due to the approximation of the Fermi surface as a sphere and the disregard of additional s-d transitions in transition metals which reduce the mean free path [38]. Also, the value of $R_{2.5}$ may be lowered by assuming a higher effective spin.

3. Results and discussion

Strontium ferromolybdate Sr_2FeMo6-d (SFMO) is a half-metallic, ferrimagnetic compound with a saturation magnetization of 4 μ_B/f.u [28]. However, SFMO does not exhibit a general metallic conductivity mechanism. In the absence of a magnetic field, the temperature dependence of conductivity of SFMO ceramics [28] is well described by the fluctuation-induced tunneling (FIT) model [39], e.g., by the presence of conducting grains separated by nanosized energy barriers where large thermal voltage fluctuations occur when the capacitance of an intergrain junction is in the order of 0.1 fF. Here, tunneling occurs between large metallic grains via the intergrain junctions with a

Preprints (www.preprints.org) | NOT PEER-REVIEWED | Posted: 16 May 2023 doi:10.20944/preprints202305.1081.v1

width w and area A. The FIT model is specified by three parameters [39]: (i) The temperature T_1 characterizing the electrostatic energy of a parabolic potential barrier,

$$kT_1 = \frac{A \cdot w \cdot \varepsilon_o E_0^2}{2}, \tag{21}$$

where k is the Boltzmann constant and the characteristic field E_0 is determined by:

$$E_0 = \frac{4V_0}{e \cdot w}, \tag{22}$$

(ii) the temperature T_0 representing T_1 divided by the tunneling constant,

$$T_0 = T_1 \cdot \left(\frac{\pi \chi w}{2}\right)^{-1}, \tag{23}$$

with the reciprocal localization length of the wave function

$$\chi = \sqrt{\frac{2m^* V_0}{\hbar^2}}, \tag{24}$$

where m^*_e is the effective electron mass, and (iii) the residual resistivity r_0. The resulting resistivity of this model is then given by [39]:

$$\rho(T) = \rho_0 \exp\left(\frac{T_1}{T_0 + T}\right), \tag{25}$$

In our case, the model parameters amount to T_0 = 141.1 K, T_1 = 25.6 K and $s_0 = 1/r_0$ =37.16 S/cm (cf. Figure 1). The FIT model was recently applied to intergrain tunneling in polycrystalline Sr_2CrMoO_6 and Sr_2FeMoO_6 ceramics [40], in half-metallic double-perovskite $Sr_2BB'O_6$ (BB'– FeMo, FeRe, CrMo, CrW, CrRe) ceramics [41] and in Ba_2FeMoO_6 thin films [42].

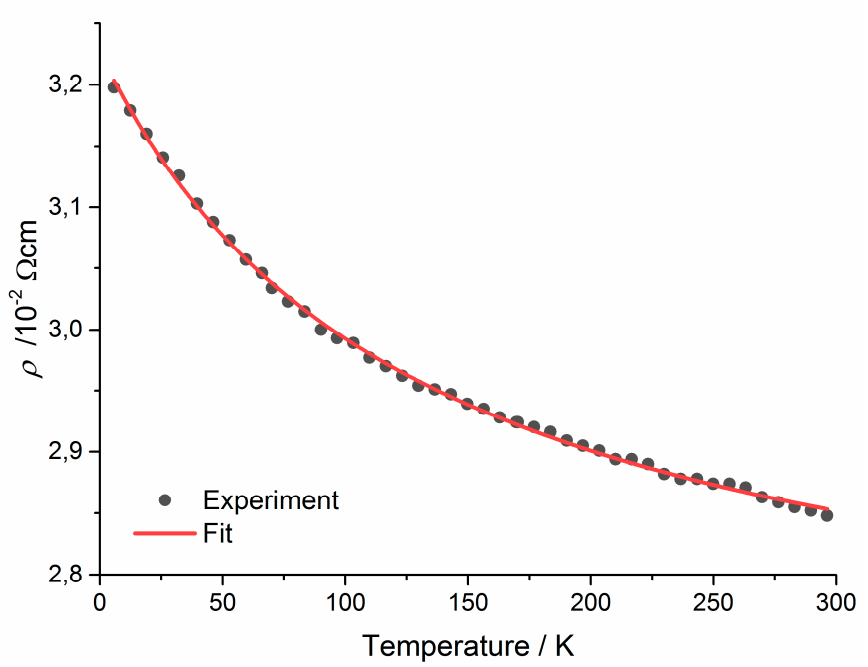

Figure 1. Fitting of the conductivity data of SFMO ceramics at zero magnetic flux [28] to the fluctuation induced tunneling model [39]. Fitting parameters are: T_0 = 141.1 K, T_1 = 25.6 K and s_0 = 37.16 S/cm.

Preprints (www.preprints.org) | NOT PEER-REVIEWED | Posted: 16 May 2023 doi:10.20944/preprints202305.1081.v1

One feature attributed to weak localization in SFMO ceramics is the decrease of resistivity in the temperature range between 405 K and 590 K [43]. In the following this resistivity behavior should be considered more in detail. According to [43], the resistivity behavior of vacuum-annealed SFMO ceramics above room temperature is separated into three regions: (i) From 300 K up to the Curie temperature of about 405 K the electrical resistivity increases with temperature and shows metallic behavior, (ii) Above 405 K up to approximately 590 K the resistivity decreases with temperature, (iii) Finally, from 590 K up to 900 K the resistivity increases since the material becomes metallic again [43].

Another report on the electrical resistivity of SFMO indicates metallic behavior up to 420 K, a decrease of resistivity in the temperature range 420–820 K, and the reversion to metallic behavior between 820 and 1120 K [44]. A similar resistivity behavior with a resistivity maximum at about 450 K, far above the Curie temperature of ~330 K [45], was obtained for Ba_2FeMoO_{6-d} while Ca_2FeMoO_{6-d} shows solely metallic behavior in the whole temperature range 320-1120 K [44].

A more detailed consideration of the reported resistivity behavior of Sr_2FeMoO_{6-d} and Ba_2FeMoO_{6-d} above T_C [43,44], reveals a convincing fit to the adiabatic small polaron hopping model [46] (Figure 2). In the small polaron model, electrical conduction of perovskites at higher temperature, i.e., above a certain transition temperature, occurs by small polarons moving through the lattice by thermally activated jumps between neighboring sites. The transition temperature from small polaron motion in a conduction band to small polaron hopping was estimated to be in the order of $\theta_D/2$ with θ_D the Debye temperature which amounts to 338 K for SFMO [47]. The adiabatic small polaron hopping model yields a resistivity of [46]:

$$\rho = \rho_0 T \exp\left(\frac{E_a}{kT}\right), \tag{26}$$

where E_a is the thermal activation energy. The obtained E_a values are 0.045-0.08 eV for $Sr_2FeMoO_{6-\delta}$ and about 0.13 eV for $Ba_2FeMoO_{6-\delta}$ and are in the order of the values of other perovskites and double perovskites: $La_{1-x}Sr_xCo_{1-y}Fe_yO_3$ [48], $Sr_{1.6}Sm_{0.4}MgMoO_{6-\delta}$, $Sr_{1.4}Sm_{0.6}MgMoO_{6-\delta}$, and $Sr_{1.2}Sm_{0.8}MgMoO_{6-\delta}$ [49], as well as $Sr_2Fe_{1.5}Mo_{0.5}O_{6-d}$ and $Sr_2Fe_{1.5}Mo_{0.5-x}Nb_xO_{6-d}$ [50].

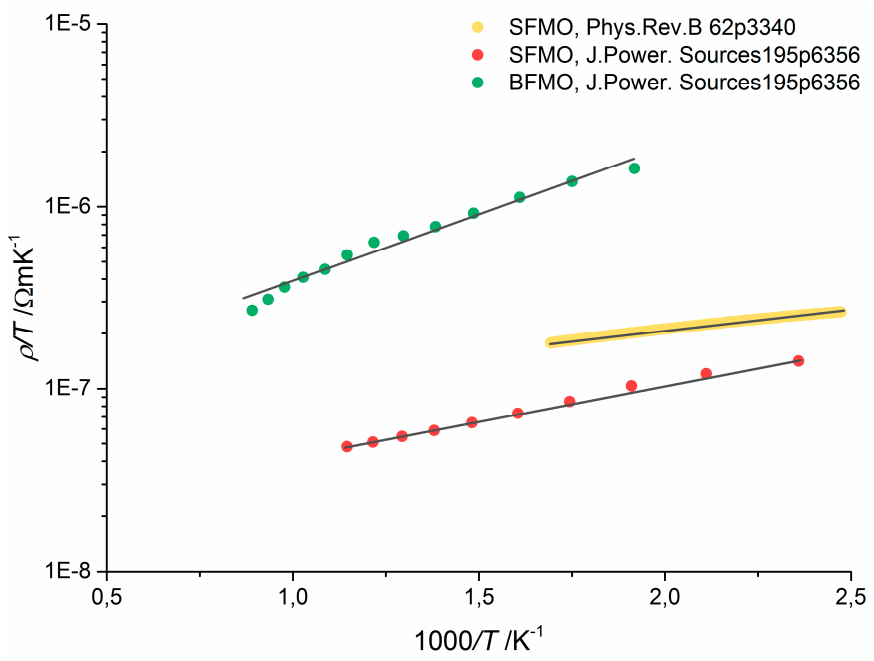

Figure 2. Fitting of the conductivity data of Sr_2FeMoO_6 ceramics between 405 K and 590 K [43] as well as of Sr_2FeMoO_6 ceramics between 420 and 870 K and Ba_2FeMoO_6 ceramics between 520 and 1120 K [44] to the adiabatic small polaron hopping model [46].

Preprints (www.preprints.org) | NOT PEER-REVIEWED | Posted: 16 May 2023 doi:10.20944/preprints202305.1081.v1

Weak localization effects were taken into account in order to explain the presence of minima in the ρ–T curves of perovskite oxides exhibiting metallic conductivity [17,19,25,51,52]. It has been suggested [20,21] that the resistivity minimum and, consequently, the resistivity upturn at lower temperature arises from the competition of two contributions—one, usual, increasing and the other, decreasing with the increase of the temperature. In eq. (15), the corresponding terms are $(B'\ln T)^{-1}$ and C_nT^n, respectively. The resistivity versus temperature plots of SFMO ceramics in a magnetic field [28] are very similar to the ones of $La_{0.7}Ca_{0.3}MnO_3$and $La_{0.7}Sr_{0.3}MnO_3$ thin films [17,19]. Also here, a resistivity minimum appears in polycrystalline SFMO ceramics at low temperature [28] which was explained by weak localization [52]. In this case, a quantum correction terms $A_WT^{p/2}$ [17,52] was added to the residual resistivity s_0 and an electron interaction term A_pT^n to the resistivity. A similar approach was applied to perovskite ceramics ($LaNi_xCo_{1-x}O_3$ and $Na_xTa_yW_{1-y}O_3$ [53], $La_{0.5}Pb_{0.5}MnO_3$ and $La_{0.5}Pb_{0.5}MnO_3$ ceramics containing 10 at.% Ag in a dispersed form [15].

To evaluate the origin of the low temperature resistivity minimum in SFMO, we fitted the experimental data [28] to eq. (15) assuming $A'= 0$ (Figure 3, Table 1). The increase of the $s_0(B)$ values correspond to a negative magnetoresistance obtained in ferrimagnetic SFMO ceramics which arises due to the suppression of spin disorder by the magnetic field [27,28,43]. The fitted s_0 values describe a power law magnetic flux dependence of the magnetoresistance, $-MR \propto B^m$, with a power of m = 0.284. This value lies in-between the values of m = 0.5 for metallic behavior and electron-electron interaction in the temperature range between the temperature of minimum resistivity and the Curie temperature and m = 0.1 for semiconducting conductivity behavior, both at high magnetic fluxes [54]. The fitted B' values are three orders of magnitude lower than the ones calculated above. Consequently, the elastic scattering time should be reduced by six orders of magnitude. This is physically nonsense. Also, the C_nT^n term does not correspond to physically meaningful quantities. The values of the exponent n cannot be attributed to a certain electron scattering mechanism. On the other hand, electron scattering should sufficiently change in dependence on the magnetic flux. When assuming n = 2 for electron-electron scattering, and taking the value $C_n = 2.16\times10^{-11}$ WmK^{-2} from [33], the fit becomes of much worse quality (Figure 4). Here, a satisfactory fit occurs only for B = 0. Assuming n = 2.5 and taking the value C_n of eq. (20), the fit is even worse with a no satisfactory fit even for B = 0.

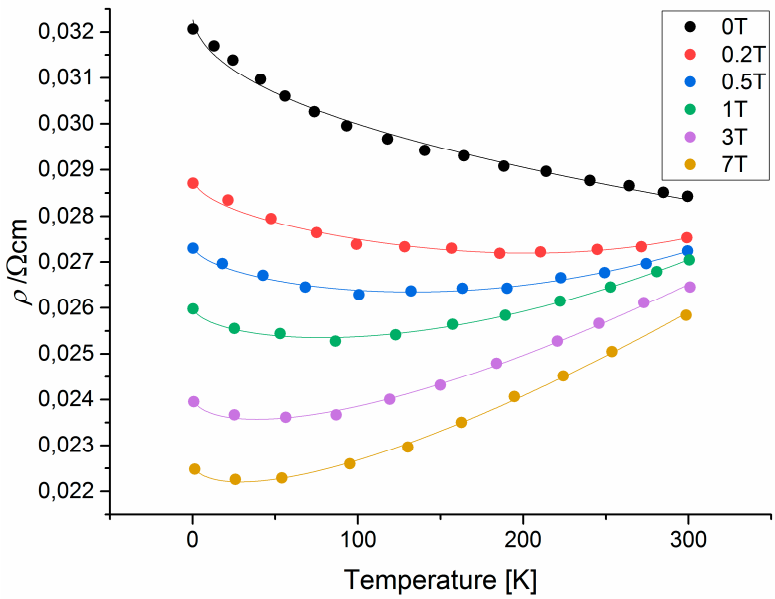

Figure 3. Fit of the conductivity data of Sr_2FeMoO_6 [28] to eq. (15) assuming $A'= 0$.

Preprints (www.preprints.org) | NOT PEER-REVIEWED | Posted: 16 May 2023 doi:10.20944/preprints202305.1081.v1

Table 1. Fit of the parameters of eq. (15) assuming A'=0 to experimental data in [28].

B, T	s_0, Sm^{-1}	B', $Sm^{-1}K^{-1/2}$	C_n, WmK^{-n}	n
0	3087	0.222	-1.37×10^{-5}	0.61
0.2	3464	0.174	6.09×10^{-12}	3.31
0.5	3649	0.161	3.75×10^{-9}	2.29
1	3839	0.166	1.15×10^{-7}	1.77
3	4150	0.235	2.21×10^{-6}	1.34
7	4414	0.270	3.73×10^{-6}	1.22

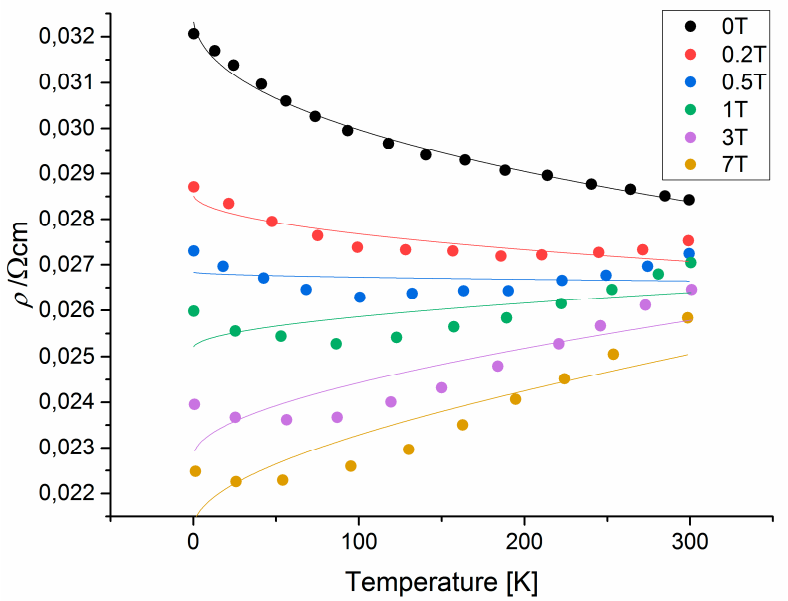

Figure 4. Fit of the conductivity data of Sr_2FeMoO_6 [28] to eq. (15) assuming A' = 0, $C_n = 2.16\times10^{-11}$, n = 2.

Thus, the only possible conclusion is that the resistivity upturn at low temperatures in Sr_2FeMoO_6 ceramics cannot be modeled by the weak localization correction due to quantum interference. Note that neither fluctuation induced tunneling nor adiabatic small polaron hopping provide favored conditions for quantum interference of back-scattered electrons.

4. Conclusions

We have related the temperature dependence of the SFMO resistivity in the absence of a magnetic field to the fluctuation induced tunneling model. The decrease in resistivity above the resistivity maximum around Curie temperature was attribute to adiabatic small polaron hopping instead to localization effects. Both fluctuation induced tunneling and adiabatic small polaron hopping do not favor quantum interference. This is evidenced by the observation that the resistivity upturn behavior of SFMO cannot be explained by weak localization. Consequently, to the best of our knowledge, there is still no convincing evidence for the presence of weak localization in SFMO.

Author Contributions: Conceptualization, G.S.; methodology, G.S; software, E.A; validation, G.S. and E.A.; formal analysis, G.S.; investigation, G.S. and E.A..; resources, G.S.; data curation, E.A.; writing—original draft preparation, G.S.; writing—review and editing, E.A..; visualization, E.A..; supervision, G.S.; project administration, G.S.; funding acquisition, G.S. All authors have read and agreed to the published version of the manuscript.

Funding: This work was funded by the EU project H2020-MSCA-RISE-2017-778308- SPINMULTIFILM.

Institutional Review Board Statement: Not applicable.

Informed Consent Statement: Not applicable.

Preprints (www.preprints.org) | NOT PEER-REVIEWED | Posted: 16 May 2023 doi:10.20944/preprints202305.1081.v1

Data Availability Statement: The original contributions presented in the study are included in the article/supplementary material, further inquiries can be directed to the corresponding author.

Acknowledgments: The authors thank Prof. N. Sobolev (University Aveiro) for valuable discussions on the topic of this work.

Conflicts of Interest: The authors declare no conflict of interest.

References

1. Akkermans. A., G. Montambaux, G. *Mesoscopic Physics of Electrons and Photons*. Cambridge University Press, Great Britain, 2007).
2. Aleiner, I.L.; Altshuler, B.L.; Gershenson, M.E. Interaction effects and phase relaxation in disordered systems, *Waves Random Media* **1999**, *9(2)*, 201-239, DOI: 10.1088/0959-7174/9/2/308.
3. Senz,. V., Quantum transport in interacting two-dimensional systems, PhD thesis, ETH, Zürich (Switzerland), March 2002, p.25. DOI: 10.3929/ethz-004320956.
4. Abrikosov, A. *Fundamentals of the theory of metals*, Elsevier, Amsterdam, Netherlands, 1988, p.213.
5. Altshuler, B.L.; Aronov, A.G.; Khmelnitzky D.E. Effects of electron-electron collisions with small energy transfers on quantum localization. *J. Phys. C: Solid State Phys*. **1982**, *15(36)*, 7367-7386, DOI: 10.1088/0022-3719/15/36/018.
6. Xu, G.; Wang, W.; Zhang, X.; Du, Y.; Liu, E.; Wang, S.; Wu, G.; Liu, Z.; and Zhang, X.X. Weak Antilocalization Effect and Noncentrosymmetric Superconductivity in a Topologically Nontrivial Semimetal LuPdBi, *Sci Rep*. **2014**, 4, 5709-7pp DOI: 10.1038/srep05709.
7. Shrestha, K.; Chou, M.; Graf, D.; Yang, H.D.; Lorenz, B. Chu, C.W. Extremely large nonsaturating magnetoresistance and ultrahigh mobility due to topological surface states in the metallic Bi_2Te_3 topological insulator. *Phys. Rev. B - Condens. Matter Mater. Phys*. **2017**, 95, 195113, DOI: 10.1103/PhysRevB.95.195113.
8. Lin, J.J.: Bird, J.P. Recent experimental studies of electron dephasing in metal and semiconductor mesoscopic structures. *J. Phys.: Condens. Matter* **2002**, *14(18)*, R501-R596, DOI: 10.1088/0953-8984/14/18/201.
9. Rammer, J.; Schmid, A. Destruction of phase coherence by electron-phonon interactions in disordered conductors, *Phys. Rev. B - Condens. Matter Mater. Phys*. **1986**, *34(2)*, 1352-1355, DOI. 10.1103/PhysRevB.34.1352.
10. Sahnoune A.; Strom-Olsen, J.O. Weak localization and enhanced electron-electron interaction in amorphous $Ca_{70}(Mg,Al)_{30}$, *Phys. Rev. B - Condens. Matter Mater. Phys*., **1989**, *39(11)*, 7561-7566, DOI: 10.1103/PhysRevB.39.7561.
11. Zhao, B.; Cheng, P.; Pan, H.; Zhang, S.; Wang, B.; Wang, G.; Xiu F.; Song, F., Weak antilocalization in Cd_3As_2 thin films. *Sci. Rep*. **2016**, *6*, 22377, DOI:10.1038/srep22377.
12. Islam, S.; Bhattacharyya, S.; Nhalil, H.; Banerjee, M.; Richardella, A.; Kandala, A.; Sen, D.; Samarth, N.; Elizabeth, S.; Ghosh A., Low-temperature saturation of phase coherence length in topological insulators, *Phys. Rev. B - Condens. Matter Mater. Phys*. **2019**, *99*, 245407 DOI: 10.1103/PhysRevB.99.245407.
13. Dey, R.; Pramanik, T.; Roy, A.; Rai, A.; Guchhait, S.; Sonde, S.; Movva, H.C.P.; Colombo, L.; Register, L.F.; Banerjee, S.K. Strong spin-orbit coupling and Zeeman spin splitting in angle dependent magnetoresistance of Bi_2Te_3, *Appl. Phys. Lett*. **2014**, 104, 223111, DOI: 10.1063/1.4881721.
14. Mathew, R.J.; Inbaraj, C.R.P.; Sankar, R.; Hudie, S.M.; Nikam, R.D.; Tseng, C.-A.; Lee C.-H.; Chen, Y.-T. High unsaturated room-temperature magnetoresistance in phase-engineered $Mo_xW_{1-x}Te_{2+d}$ ultrathin films, *J. Mater. Chem. C* **2019**, *7*, 10996, DOI: 10.1039/c9tc02842k.
15. Rozenberg, E.; Auslender, M.; Felner, I.; Gorodetsky, G. Low-temperature resistivity minimum in ceramic manganites. *J. Appl. Phys*. **2000**, *88(5)*, 2578-2582, DOI: 10.1063/1.1288704.
16. Herranz, G.; Martínez, B.; Fontcuberta, J.;. Sánchez, F.; Ferrater, C.; García-Cuenca, M.V.; Varela, M. Enhanced electron-electron correlations in nanometric $SrRuO_3$ epitaxial films, *Phys. Rev. B - Condens. Matter Mater. Phys*. **2003**, 67, 174423, DOI: 10.1103/PhysRevB.67.174423.
17. Maritato, L.; Adamo, C.; Barone, C.;. De Luca, G.M ; Galdi, A.; Orgiani, P.; Petrov, A.Yu. Low-temperature resistivity of $La_{0.7}Sr_{0.3}MnO_3$ ultra thin films: Role of quantum interference effects. *Phys. Rev. B - Condens. Matter Mater. Phys*. **2006**, *73*, 094456. DOI: 10.1103/PhysRevB.73.094456
18. Lee, P.A.; Ramakrishnan, T.V. Disordered electronic systems, *Rev. Mod. Phys*. **1985**, *57(2)*, 287-337, DOI: 10.1103/RevModPhys.57.287.
19. Kumar, D.; Sankar, J.; Narayan, J.; Singh R.K.; Majumdar, A.K., Low-temperature resistivity minima in colossal magnetoresistive $La_{0.7}Ca_{0.3}MnO_3$ thin films. *Phys. Rev. B - Condens. Matter Mater. Phys*. **2002**, *65*, 094407, DOI: 10.1103/PhysRevB.65.094407.
20. Kondo, J. Resistance minimum in dilute magnetic alloys, *Prog. Theor. Phys*. **1964**, *32*, 37-49, DOI: 10.1143/PTP.32.37.
21. Barman, A.; Ghosh, M.; Biswas, S.; De S.K.; Chatterjee, S . Electrical and magnetic properties of $La_{0.7-x}Y_xSr_{0.3}MnO_3$ ($0 \le x \le 0:2$) perovskite at low temperature, *J. Phys.: Condens. Matter* **1998**, *10(43)*, 9799–9811, DOI 10.1088/0953-8984/10/43/024.

Preprints (www.preprints.org) | NOT PEER-REVIEWED | Posted: 16 May 2023 doi:10.20944/preprints202305.1081.v1

22. Tiwari, A.; Rajeev, K.P. Low-temperature electrical transport in $La_{0.7}A_{0.3}MnO_3$, (A: Ca, Sr, Ba), *Solid State Commun*. **1999**, *111(1)*, 33–37, DOI: 10.1016/S0038-1098(99)00148-9.
23. Barman, A., Ghosh, M., Biswas, S.,. De, S.K:, Chatterjee, S. Electrical properties of $La_{0.6}Re_{0.1}Ca_{0.3}MnO_3$ (Re=Pr, Sm, Gd, Dy) at low temperature, *Solid State Commun*. **1998**, *106(10)*, 691–694, DOI: 10.1016/S0038-1098(98)00106-9.
24. Herranz, G.; Sánchez, F.; Martínez, B.; Fontcuberta, J.; García-Cuenca, M. V.; Ferrater, C.; Varela, M.; Levy, P. Weak localization effects in some metallic perovskites. *Eur. Phys. J. B* **2004**, 40, 439–444, DOI: 10.1140/epjb/e2004-00207-9.
25. Herranz, G.; Sánchez, F.; Fontcuberta, J.; Laukhin, V.; Galibert, J.; García-Cuenca, M.V.; Ferrater, C.; Varela, M. Magnetic field effect on quantum corrections to the low-temperature conductivity in metallic perovskite oxides *Phys. Rev. B - Condens. Matter Mater. Phys*., **2005**, *72*, 014457 DOI: 10.1103/PhysRevB.72.014457.
26. Raychaudhuri, A.K.; Rajeev K.P.;, Srikanth, H.; Mahendiran, R. Low temperature studies on normal perovskite oxides: role of correlation and disorder, *Physica B: Condens. Mat*., **1994**, *197(1-4)*, 124-132, DOI: 10.1016/0921-4526(94)90206-2.
27. Westerburg, W. Spinpolarisierter Transport in epitaktischen Manganoxid und Doppelperowskitschichten, Ph.D. Thesis, Universität Mainz, October 6th, 2000.
28. Kobayashi, K.I.; Kimura, T.; Sawada, H.; Terakura, K.; Tokura, Y. Room-Temperature Magnetoresistance in an Oxide Material with an Ordered Double-Perovskite Structure. *Nature* **1998**, *395*, 677–680, doi:10.1038/27167
29. B. Knook, De anomale electrische Weerstand van een aantal Cu-, Ag-, en Au-Legeringen, PhD Thesis, University of Leiden, Netherlands, April 4th, 1962.
30. Mazur, D.; Gray, K. E.; Zasadzinski, J.F.; Ozyuzer, L.; Beloborodov, I.S.; Zheng, H.; Mitchell, J.F. Redistribution of the density of states due to Coulomb interactions in $La_{2-2x}Sr_{1+2x}Mn_2O_7$, *Phys. Rev. B - Condens. Matter Mater. Phys*., 76, **2007**, 193102, DOI: 10.1103/PhysRevB.76.193102.
31. Nath, T. K.; Majumdar A. K. Quantum interference effects in $(Ni_{0.5}Zr_{0.5})_{1-x}Al_x$ metallic glasses, *Phys. Rev. B - Condens. Matter Mater. Phys*., **2007**, *55(9)*, 5554-5557, DOI: . 10.1103/PhysRevB.55.5554.
32. Cochrane, R.W.; Strom-Olsen J.O. Scaling behavior in amorphous and disordered metals, *Phys. Rev. B - Condens. Matter Mater. Phys*. **1984**, *29(2)*, 1088-1090, DOI: 10.1103/PhysRevB.29.1088.
33. Tomioka, Y.; Okuda, T.; Okimoto, Y.; Kumai, R.; Kobayashi, K.; Tokura, Y. Magnetic and Electronic Properties of a Single Crystal of Ordered Double Perovskite. *Phys. Rev. B - Condens. Matter Mater. Phys*. **2000**, *61(1)*, 422-427, doi:10.1103/PhysRevB.61.422.
34. Yanagihara, H.; Salamon, M.B.; Lyanda-Geller, Y.; Xu, S.; Moritomo, Y. Magnetotransport in double perovskite Sr_2FeMoO_6: Role of magnetic and nonmagnetic disorder. *Phys. Rev. B - Condens. Matter Mater. Phys*. **2001**, *64*, 214407, DOI: 10.1103/PhysRevB.64.214407.
35. Dyson, F.J., General Theory of Spin-Wave Interactions, *Phys. Rev*. **1956**, 102(5), 1217-1230, DOI: 10.1103/PhysRev.102.1217.
36. Motida K.; Miyahara, S. On the 90° exchange interaction between cathions (Cr^{3+}, Mn^{2+}, Fe^{3+} and Ni^{2+}) in oxides, *J. Phys. Soc. Jpn*. **1970**, *28(5)*, 1188-1196, DOI: 10.1143/JPSJ.28.1188.
37. Voogt, F.C.; Palstra, T.T.M.; Niesen, L.; Rogojanu, O.C.; James, M. A.; Hibma T. Superparamagnetic behavior of structural domains in epitaxial ultrathin magnetite films *Phys. Rev. B - Condens. Matter Mater. Phys*. **1998**, *57(14)*, R8107-R8110, DOI: 10.1103/PhysRevB.64.214407.
38. Suchaneck, G.; Artiukh, E.; Gerlach, G. Resistivity and tunnel magnetoresistance in double-perovskite strontium ferromolybdate ceramics, *Physica Status Solidi B*, **2022**, *259(8)*, 2200012, (10 pp), DOI: 10.1002/pssb.202200012.
39. Sheng, P.; Sichel, E.K. ; Gittleman, J.I. Fluctuation-induced tunneling conduction in carbon-polyvinylchloride composites, *Phys. Rev. Lett*. **1978**, *40(18)*, 1197–2000, doi:10.1103/PhysRevLett.40.1197.
40. Fisher, B.; Genossar, J.;. Chashka, K.B ; Patlagan, L.; Reisner, G.M. Remarkable power-law temperature dependencies of inter-grain conductivity, *Solid State Commun*. **2006**, *137(12)*, 641–644, doi:10.1016/j.ssc.2006.01.032.
41. Fisher, B.; Genossar, J.; Chashka, K.B.; Patlagan, L.; Reisner, G.M. Inter-grain tunneling in the half-metallic double-perovskites $Sr_2BB'O_6$(BB'= FeMo, FeRe,CrMo, CrW, CrRe), *Proceedings of the EPJ Web of Conferences*, **2014**, 75, 01001, DOI: https://doi.org/10.1051/epjconf/20147501001.
42. S. Granville, I.L. Farrell, A.R. Hyndman, D.M. McCann, R.J. Reeves, G.V.M. Williams, Indications of spin polarized transport in Ba_2FeMoO_6 thin films, (2017). Available online: http://arxiv.org/abs/1707.01208, accessed on April 14th, 2023.
43. Niebieskikwiat, D.; Sánchez, R.; Caneiro, A.; Morales, L.; Vásquez-Mansilla, M.; Rivadulla, F.; Hueso, L. High-Temperature Properties of the Double Perovskite: Electrical Resistivity, Magnetic Susceptibility, and ESR. *Phys. Rev. B - Condens. Matter Mater. Phys*. **2000,** *62(2)*, 3340–3345, DOI:10.1103/PhysRevB.62.3340.
44. Zhang, L.; Zhou, Q.; He, Q.; He, T. Double-Perovskites $A_2FeMoO_{6-\delta}$ (A = Ca, Sr, Ba) as Anodes for Solid Oxide Fuel Cells. *J. Power Sources* **2010**, *195(19)*, 6356–6366, doi:10.1016/j.jpowsour.2010.04.021.

Preprints (www.preprints.org) | NOT PEER-REVIEWED | Posted: 16 May 2023 doi:10.20944/preprints202305.1081.v1

45. Maignan, A.; Raveau, B.; Martin, C.; Hervieu, M. Large Intragrain Magnetoresistance above Room Temperature in the Double Perovskite Ba_2FeMoO_6. *J. Solid State Chem.* **1999**, 144, 224–227, DOI: 10.1006/jssc.1998.8129.
46. Emin, D.; Holstein, T. Studies of Small-Polaron Motion IV. Adiabatic Theory of the Hall Effect. *Ann. Phys.* **1969**, *53*, 439–520, doi:10.1016/0003-4916(69)90034-7.
47. Okuda, T.; Kobayashi, K.-I.; Tomioka, Y.; Tokura, Y. Anomalous low-temperature specific heat around the metal-insulator transition in ordered double-perovskite alloys $Sr_2Fe(Mo_{1-y}W_y)O_6$ ($0 \le y \le 1$), *Phys. Rev. B - Condens. Matter Mater. Phys.* **2003**, 68, 144407, DOI: 10.1103/PhysRevB.68.144407.
48. Tai, L.W.; Nasrallah, M.M.; Anderson, H.U.; Sparlin, D.M.; Sehlin, S.R. Structure and Electrical Properties of $La_{1-x}Sr_xCo_{1-y}Fe_yO_3$. Part 2. The System $La_{1-x}Sr_xCo_{0.2}Fe_{0.8}O_3$. *Solid State Ionics* 1995, *76(3-4)*, 273–283, DOI:10.1016/0167-2738(94)00245-N.
49. Zhang, L.; He, T. Performance of Double-Perovskite $Sr_{2-x}Sm_xMgMoO_{6-\delta}$ as Solid-Oxide Fuel-Cell Anodes. *J. Power Sources* **2011**, *196(20)*, 8352–8359, DOI:10.1016/j.jpowsour.2011.06.064.
50. Hou, M.; Sun, W.; Li, P.; Feng, J.; Yang, G.; Qiao, J.; Wang, Z.; Rooney, D.; Feng, J.; Sun, K. Investigation into the Effect of Molybdenum-Site Substitution on the Performance of $Sr_2Fe_{1.5}Mo_{0.5}O_{6-\delta}$ for Intermediate Temperature Solid Oxide Fuel Cells. *J. Power Sources* **2014**, *272*, 759–765, DOI:10.1016/j.jpowsour.2014.09.043.
51. Auslender, M.; Kar'kin, A.E.; Rozenberg, E. Low-temperature resistivity minima in single-crystalline and ceramic $La_{0.8}Sr_{0.2}MnO_3$: Mesoscopic transport and intergranular tunneling, *J. Appl. Phys*. **2001**, *89(11)*, 6639-6641; DOI: 10.1063/1.1357140.
52. Kalanda, N.; Demyanov, S.; Yarmolich, M.; Petrov, A.; Sobolev N.; Electric transport characteristics of $Sr_2FeMoO_{6-\delta}$ ceramics with structurally inhomogeneous surfaces, In: Workshop book, 2nd International Workshop on Advanced Magnetic Oxides (IWAMO), November 24-25, Aveiro, Portugal, 2021, p.24.
53. Raychaudhuri, A.K. ; Rajeev, K.F. ; Srikanth, H.; Gayathri, N. Metal-insulator transition in perovskite oxides: Tunneling experiments, *Phys. Rev. B - Condens. Matter Mater. Phys*. **1995**, *51(12)*, 7421-7428, DOI: 10.1103/PhysRevB.51.7421.
54. Saloaro, M.; Majumdar, S.; Huhtinen H.; Paturi P. Absence of traditional magnetoresistivity mechanisms in Sr_2FeMoO_6 thin films grown on $SrTiO_3$, MgO and $NdGaO_3$ substrates, *J. Phys.: Condens. Matter* **2012**, 24, 366003 (9pp), DOI: :10.1088/0953-8984/24/36/366003.

Disclaimer/Publisher's Note: The statements, opinions and data contained in all publications are solely those of the individual author(s) and contributor(s) and not of MDPI and/or the editor(s). MDPI and/or the editor(s) disclaim responsibility for any injury to people or property resulting from any ideas, methods, instructions or products referred to in the content.